Articles

Polyproline II Helix Is a Key Structural Motif of the Elastic PEVK Segment of Titin

Kan Ma,[‡] Lou-sing Kan,[§] and Kuan Wang*,[‡]

Laboratory of Physical Biology, National Institute of Arthritis and Musculoskeletal and Skin Diseases, National Institutes of Health, Bethesda, Maryland, USA 20892, and Institute of Chemistry, Academia Sinica, Taipei, Taiwan, ROC

Received September 28, 2000; Revised Manuscript Received January 2, 2001

ABSTRACT: Titin is a family of giant elastic proteins that constitute an elastic sarcomere matrix in striated muscle. In the I-band region of the sarcomere, where titin extends and develops passive force upon stretch, titin is composed of tandem repeats of ∼100 residue immunoglobin domains and ∼28-residue PEVK modules. We have performed 2D NMR and circular dichroism (CD) studies of the conformations of one representative 28-mer PEVK module from human fetal titin (PEPPKEVVPEKKAPVAPPKKPEVPPVKV). NMR data of synthetic peptides of this module as well as three constituent peptides of 9 to 12 residues in aqueous solutions reveal distinguishing features for left-handed three-residue per turn PPII helices: the lack of NOE NN(i, i+1), very large NOE αN(i, i+1)/NN(i, i+1), no medium range NOE αN(i, i+2), and dihedral angles ϕ and ψ values of −78 and 146, respectively. Structural determinations indicate the presence of three short stretches of PPII helices of 4, 5, and 6 residues that are interposed with an unordered, and presumably flexible, spacer region to give one "polyproline II helix-coil" or "PhC" motif for roughly every 10 residues. These peptides also display the characteristic PPII CD spectra: positive peak or negative shoulder band at 223 nm, negative CD band near 200 nm, and biphasic thermal titration curves that reflect varied stability of these PPII helices. We propose that this PhC motif is a fundamental feature and that the number, length, stability, and distribution of PPII is important in the understanding of the elasticity and protein interactions of the PEVK region of titin.

Titin is a family of giant elastic proteins that constitute an elastic matrix in the striated muscle sarcomeres. These modular proteins may play pivotal roles in the genesis of long range elasticity, in the maintenance of sarcomere stability, and in the assembly of nascent sarcomeres of developing cells. The sequence of muscle titin encodes a blueprint for the architecture of the sarcomere and the guiding principles for the generation of tissue-specific elasticity (for recent reviews, see refs *1*−*3*).

In the skeletal and cardiac muscles, each titin molecule spans half a sarcomere from the M line to the Z line, associates with myosin thick filaments along most of its length, and connects the thick filaments to the Z line via an extensible I band segment. The extension of this elastic connector in the I band generates the restoring force (passive tension) when resting muscle is stretched (*4*, *5*).

The defining characteristics of passive tension curve are mainly the total lengths of the extensible segment, the degree of stretch, their respective elastic properties, and strength of interaction with thick filaments and the Z lines (*4*, *5*). In the I-band region, where titin extends during passive force development, titin is composed of serial-linked motifs of three types: (i) the folded 100-residue modular repeats of immunoglobin (Ig) or fibronectin (Fn3) domains, (ii) a unique PEVK[1] motif that consists of 70% of proline, glutamate, valine, and lysine residues, and (iii) the N2-A or N2-B insert (*6*). Tissue- and species-specific alternative splicing alters the expression of these motifs (*6*, *7*). The resulting change in titin in turn produces unique passive force-extension curves that can be scaled to one master relationship (*4*, *8*).

To evaluate molecular theories of titin elasticity, detailed knowledge of the conformation and stability of different

* Address correspondence to Dr. Kuan Wang, B6/Rm 401, LPB, NIAMS, NIH, Bethesda, MD 29892, 301-496-4097 (phone), 301-402-8566 (fax), wangk@exchange.nih.gov.

[‡] National Institutes of Health.

[§] Academia Sinica.

[1] Abbreviations: CD: circular dichroism; CSI: chemical shift index; CVFF: consistent valence force field; DQF-COSY: double quantum filtered correlation spectroscopy; MALDI-TOF: matrix-assisted laser desorption ionization time-of-flight mass spectroscopy; NMR: nuclear magnetic resonance; NOE: nuclear Overhauser effect; NOESY: nuclear Overhauser effect spectroscopy; PEVK: a titin segment that consists mainly of proline, glutamate, valine, and lysine; PhC: poly proline II helix-coil motif; PPII: poly proline II left-handed helix; PR: a 28-mer sequence module of PEVK; PR1, PR2, PR3: subfragments of PR; RP-HPLC: reverse phase high-pressure liquid chromatograph; TP1: a 53-kDa PEVK fragment of human fetal skeletal muscle titin; RMSD: root-mean-square deviation; ROESY: rotating frame NOESY; TOCSY: total correlation spectroscopy.

10.1021/bi0022792 CCC: $20.00
Published on Web 02/27/2001

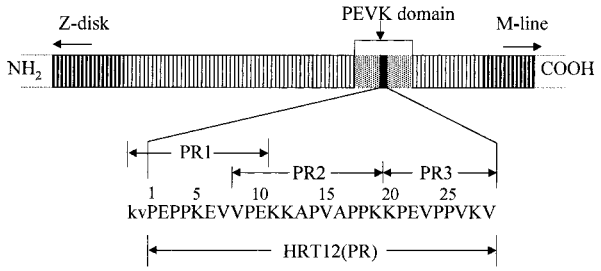

FIGURE 1: PEVK segment, PEVK module, and three PEVK peptides. PEVK segment of the giant elastic protein titin is located in the I band region of the sarcomere of skeletal and cardiac muscles. One of the many tandem repeats of ~28-residue PEVK module of human fetal skeletal muscle titin (HRT12, designated as PR, 28-mer) and three subpeptides, PR1 (12-mer), PR2 (12-mer), and PR3 (9-mer) were synthesized and investigated in this work. Note that two residues from the C-terminus of the previous module (kv in lower cases) were added at the N-terminus of PR1.

classes of titin domains is essential. It is widely assumed that PEVK has little regular structure and that an entropy-based molecular spring can explain titin elasticity (*6*, *9*, *10*). Recent structural studies from this laboratory have raised questions on the validity of this notion. Wang and co-workers (*11*) reported an initial sequence and molecular analysis of the PEVK of human fetal skeletal muscle titin. The open reading frame of a 2.5-kb cDNA clone was found to consist of tandem repeats of a fundamental PEVK module that averages 28 residues. Conformational and hydrodynamic studies of a 16 PEVK module (469 residue) expressed protein, designated as TP1, have shown that TP1 is an open and flexible chain with stable structural folds. Conformational studies by circular dichroism indicate the likely presence of polyproline II type of left-handed helices in TP1. Further examination of this and other PEVK sequences of titin revealed the presence of numerous PXXP motif (e.g., PVAP) that is frequently found in polyproline II-like (PPII) left-handed helices. This analysis suggests that PPII may indeed be a major structural motif of PEVK in titin.

To further explore this proposal, we undertook detailed NMR and CD studies of one representative PEVK module from human fetal titin. Synthetic peptides of this 28-residue PEVK module (PEPPKEVVPEKKAPVAPPKKPEVPPVKV, designated as PR) as well as three subfragments (PR1, PR2, and PR3) (Figure 1) were examined by 2D NMR and CD to search for supporting evidence of PPII helices. NMR studies revealed the presence of three PPII type of helices that are 3 residues per left-handed turn with ϕ and ψ angles restricted to the regions −78 and +146, respectively. The CD spectra and the thermal titration of these peptides are all accountable by the characteristic behavior of polyproline II helices. We propose that tandem repeats of this "polyproline helix-coil (PhC)" motif are fundamental structural features of the PEVK region of titin.

MATERIALS AND METHODS

Peptide Synthesis and Purification. A 28-residue PEVK module (PEPPKEVVPEKKAPVAPPKKPEVPPVKV), corresponding to residues 386−413 (HRT12) from the open reading frame HFT11 of human fetal skeletal titin (*11*), was selected as a representative PEVK module (Figure 1). The peptide (PR), including three fragments: PR1 (KVPEPPKEVVPE, 12-mer), PR2 (VPEKKAPVAPPK, 12-mer), and PR3 (KPEVPPVKV, 9-mer) were synthesized by Sigma-Genosys and further purified in this lab using RP-HPLC with a C-18 Phenomenex column (250 × 10 mm). The peptide (1 mg in water) was eluted with a linear gradient of 0−100% buffer B in 60 min (A: 0.1% TFA in water, B: 0.1% TFA in acetonitrile) at a flow rate of 1 mL/min at room temperature. The purity of the peptides was confirmed by analytical HPLC and electrospray mass spectroscopy and matrix-assisted laser desorption ionization time-of-flight mass spectroscopy (MALDI-TOF). The calculated and observed molecular masses were PR, calculated 3011.7, experimental 3011.9; PR1, calculated 1347.6, experimental 1347.6; PR2, calculated 1260.5, experimental 1260.9; and PR3, calculated 992.2, experimental 992.7.

Circular Dichroism Measurements. All spectra were obtained with the Jasco spectropolarimeter, model J-715, installed with a standard data analysis program (Jasco Inc., Tokyo, Japan). The temperature was controlled with a Peltier type temperature control system, model PTC-348WI. All synthetic PEVK peptides were soluble in aqueous solution. All solutions contained 10 mM potassium phosphate as buffer, and the pH was adjusted to 7.0 with H_3PO_4/KOH. A quartz cell of 0.1 cm path length was used. Spectra were recorded with a 1.0 nm bandwidth and resolution of 0.1 nm over the wavelength range 180 to 250 nm. A total of four scans were averaged for both sample and solvent to improve the signal/noise ratio. All spectra were obtained by subtracting buffer spectra, and no filtering or other smoothing techniques was used to reduce the noise levels. All measurements were under a constant nitrogen flow at 9 L/min to flush away oxygen, which absorbs below 200 nm. Polyproline (M_r 5000) was purchased from Sigma Chemical Co.

Nuclear Magnetic Resonance Spectroscopy. The lyophilized peptides were rehydrated in H_2O/D_2O (9:1 molar ratio) or D_2O in 10 mM sodium phosphate buffer (pH 7.0) containing 3-(trimethylsilyl)propionate-2,2,3,3-d_4 (TSP) (0.05 mM) as an internal chemical shift reference at 0 ppm. Final concentrations of 5−6 mM peptide solutions were attained. The final pH value was 6.9. The samples were stable up to 3 months as monitored by the 1D ^{1}H spectra. Deuterium oxide (D_2O) was purchased from Cambridge Isotope Laboratories, Inc.

All ^{1}H NMR spectra were obtained at 600 MHz using a Varian Unity Plus-600 spectrometer at the Cleveland Center for Structural Biology, Cleveland, OH. The NMR measurements were performed at 5, 15, 25, and 35 °C, and the carrier was placed in the center of the spectrum at the position of the H_2O signal. The H_2O signal was suppressed by either low-power irradiation or the Watergate pulse during the recycle delay. For the 1D spectra, 16 scans were acquired with a total recycle delay of 4.5 s, which included an acquisition time and recycle delay of 2.5 and 2.0 s, respectively. Typically, the digital resolution of the acquired data was 0.20 Hz/pt, which was reduced to 0.10 Hz/pt by zero-filling the data (32K points) once before processing. To further improve the resolution, spectra were multiplied by a Lorentzian-to-Gaussian weighting factor prior to Fourier transformation.

Four types of 2D NMR experiments were utilized in the studies of PEVK peptides: (i) homonuclear Hartmann−Hahn spectroscopy (HOHAHA) or total-correlation spectroscopy (TOCSY) (*12*), (ii) nuclear Overhauser enhancement spec-

troscopy (NOESY) (*13*), (iii) 2D H-H DQF-COSY (*14*), and (iv) H-H ROESY (*15*). These experiments were performed in the phase-sensitive mode with quadrature detection in both dimensions (*16*). For the majority of the experiments, the H_2O signal was suppressed by presaturation. The spectral width in both dimensions of these 2D spectra was 6600 Hz, and 256 complex increments (each consisting of 16 scans) were acquired with 2048 points for the F_1 and F_2 dimensions, respectively. The TOCSY experiment employed a DIPSI pulse sequence and was acquired with a mixing time of 60 ms (*17*). The H_2O irradiation was carried out by Watergate pulses for samples in H_2O during which the recycle delay (1.5 s) and the mixing time (150 and 300 ms) of the NOESY experiments and 150 ms of the ROESY experiments. Before Fourier transformation, spectra were multiplied by a skewed sinebell-squared window function (for TOCSY, ROESY, and DQF-COSY) and a Lorentzian-to-Gaussian window function (for NOESY) in F_2, and a 90° phase-shifted sinebell in F_1. Baseline roll was reduced by careful adjustment of the intensity of the first points in F_2 and F_1 (*18*). The coupling constant ($^3J_{\alpha N}$) values were determined from the 1D spectrum and DQF-COSY spectra with high digital resolution.

Structure Calculation. The NOESY (for PR) and ROESY (for PR1, PR2, and PR3) cross-peak intensities (mixing time 150 ms, 25 °C) were determined with the FELIX program (version 97.0, Biosym, Inc.) and converted to distance restraints. The NOEs classified as strong, medium, and weak corresponded to interproton distance restraints of 1.8−2.5, 2.5−3.5, and 3.5−5.0 Å, respectively. Cross-peaks with greater than 30% overlapped area were used as qualitative upper bound restraints of 1.8−5.0 Å, and pseudoatom corrections were used for degenerate peaks. Structures were computed using a well-established DGII method, which was part of the NMRRefine module of the INSIGHT II program (version 98.0, Biosym, Inc.). An extended polypeptide was built using the BIOPOLYMER module and then minimized with the DISCOVER program. The DGII protocol includes bound smoothing, in which triangular inequality limits are determined for distance geometry, followed by random metrization with the coordinates and the appropriate distances obtained by angular embedding and majorization procedures. The final structures are optimized by simulated annealing and conjugated gradient minimization procedures. The ϕ angle restraints obtained from $^3J_{\alpha N}$ and total of 79 NOEs for PR1, 87 NOEs for PR2, and 87 NOEs for PR3 distance restraints were used for structure calculations. These structures were subsequently subjected to restrained energy minimization and molecular dynamics. The system was first energy minimized for 500 cycles using conjugate gradients with CVFF force field (*19*) and followed by a 30 ps restrained dynamics. Then the system was heated to 650 K for 2 ps, followed by cooling to 300 K. The system was finally energy minimized with 100 cycles of steepest descent and 1500 cycles of conjugate gradient refinement.

PPII Model Building. The ideal PPII conformation model was built using the INSIGHT II program (version 98.0, Biosym, Inc.) based on ϕ and ψ values of −78 and 146, respectively. The NOE intensities were scaled relative to that expected for a fixed interproton separation of 4.5 Å (set to 1.0), intensities less than 0.3 (equivalent to a fixed distance of 5.5 Å) being set to zero. The coupling constant was calculated using the Karplus relationship (*20, 21*) with ϕ value of −78.

RESULTS

Experimental Strategy. Our previous analysis of the motifs of PEVK region indicates the presence of repeats of ∼28-residue module, superrepeats of seven module, and nonrepeat sequence (*11*). Conformational studies indicate the presence of left-handed polyproline type II helices in an expressed protein that contains all three sequence elements. It was not clear whether repeats and nonrepeats adopt the PPII conformation that is a left-handed three residue per turn helix, with ϕ and ψ angles at or near −78 and +146, respectively (*22*).

To facilitate the interpretation of NMR spectra, we also studied three component peptides (PR1, PR2, and PR3) of this module (PR). PR3 was designed based on the empirical observation that the first residue in some PPII helices is likely to be an amino acid other than Pro, with positively charge residues being most common (*23*). Therefore, the C-terminal fragment (KPEVPPVKV, designated as PR3) was designed, which starts with a positively charged Lys.

The design of PR2 was guided by our search for potential consensus SH3 binding sequences that adopt a PPII conformation (*24*). Examining our PEVK sequence revealed that VPEKKAPVAPPK (PR2) of this module appears to meet the criteria for such SH3 binding sequences. This sequence consists of three Pro (P9, P14, and P17) at positions 2, 7, and 10 with a hydrophobic residue at position 8; prolines at these positions tend to stabilize the formation of the PPII helix (*24*). In addition, residues K11, P14, and P17 could form one edge and A13 and A16 form another edge of the PPII helix that interacts with the binding pocket of SH3. We therefore suspect that PR2 might form a PPII helical conformation.

PR1 (KVPEPPKEVVPE) contains the balance of the module with three residues (VPE) overlapping with PR2 and two extra residues at its C terminus, VK, from the preceding module HRT11. These extra residues are added to avoid end effects and to facilitate structural interpretation of the NMR data.

Circular Dichroism of Polyproline and PEVK Peptides. As a standard of polyproline II left-handed helix, we measured the spectrum of poly-L-proline in phosphate buffer (Figure 2, panel A). This spectrum reproduced well the characteristic features of a stable polyproline II helix in polar environments: a strong negative band around 206 nm ($\pi-\pi^*$ transition) and a weak positive band at 229 nm ($n-\pi^*$ transition) (*25, 26*). Thermal titration of polyproline from 2 to 80 °C revealed a biphasic transition of the ellipticity at 229 nm: it decreased linearly with two distinct slopes and an intercept at 52 °C (Figure 2, panel B). These data provide a set of references for comparing the CD spectra of the PEVK peptides.

The CD spectra of PR peptide together with PR1, PR2, and PR3 peptides in phosphate buffer at 2 °C display similar characteristics of PPII helix: a strong negative band near 200 nm and a weak negative shoulder (PR, PR1, PR3) or a slightly positive band at 223 nm (PR2) (Figure 3). They differ from the polyproline spectrum in that there is a blue shift of the negative band by ∼5 nm for all peptides and the absence of the weak positive band at 223 nm expected for PPII helix

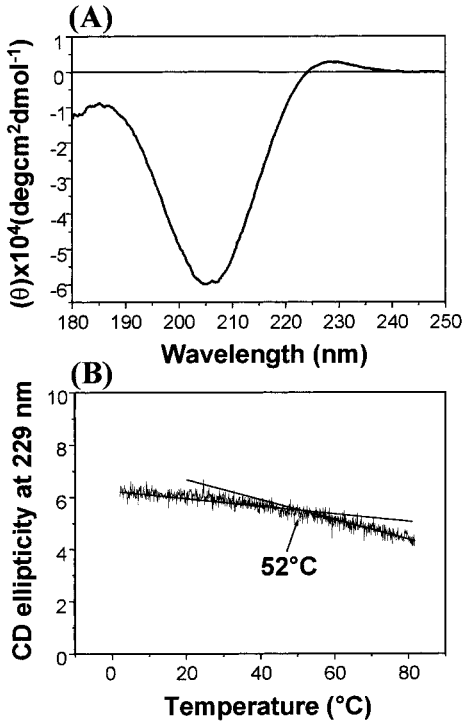

FIGURE 2: CD spectra and thermal transition of polyproline. (A) Polyproline (M_r 5000, 0.25 mg/mL) in 10 mM KPi, pH 6.9, at 2 °C exists as a PPII helix; (B) Thermal titration of polyproline was monitored by continuous measurement of CD value at 229 nm from 2 to 80 °C. Note the characteristic biphasic linear transition with an inflection point at 52 °C.

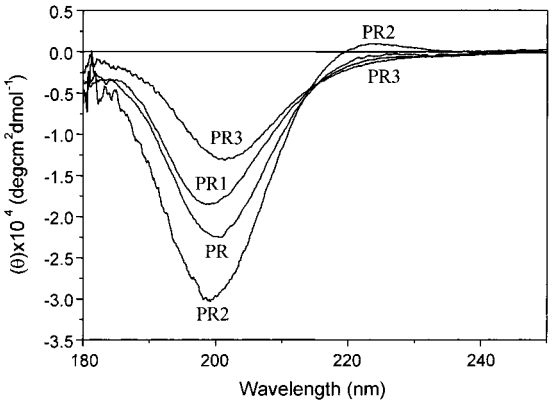

FIGURE 3: CD spectra of PR, PR1, PR2, and PR3. Peptides (0.15, 0.35, 0.4, and 0.46 mg/mL for PR, PR1, PR2, and PR3, respectively) in 10 mM KPi, pH 6.9, 2 °C were measured, and molar ellipticity (θ) per residue was plotted. Note the similarity in spectra, especially PR2, to that of polyproline.

for all but one peptide (PR2). This difference may be attributed to a slight deviation from the ideal PPII ($\phi = -78$ °C, $\varphi = 146°$, $\omega = 180°$) helical conformation (*27*). The presence of cis proline conformations may also cause a change in the positive n$-\pi^*$ transition at 229 nm and a shift in the $\pi-\pi^*$ transition at 206 nm toward shorter wavelength (*28*). Of the three peptides, the CD spectrum of PR2 displays the most striking similarity with that of polyproline: a strong negative band at 198 nm and a weak positive band near 223 nm, strongly suggesting PR2 contains substantial PPII structure. PR1 has a less intense negative band near 198 nm and a small negative shoulder at 223 nm. PR3 has the least intense negative band red-shifted ca. 3 to 201 nm and a negative shoulder at 223 nm (Figure 3). The significantly

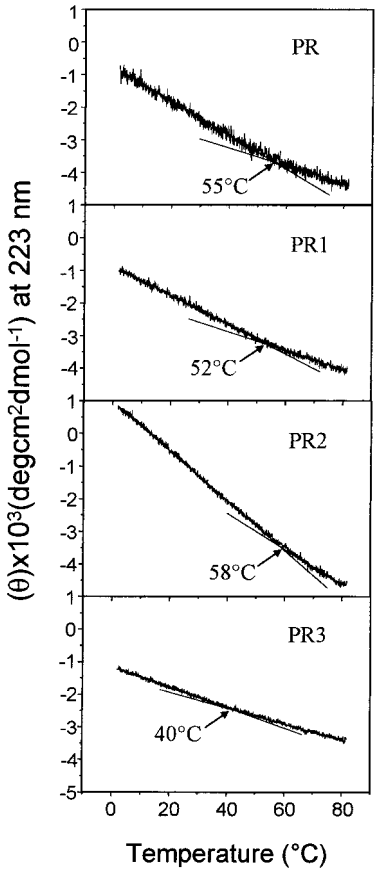

FIGURE 4: Thermal titration of PR, PR1, PR2, and PR3. Thermal titration of PR, PR1, PR2, and PR3 was monitored by continuous measurement of CD value at 223 nm from 2 to 80 °C. Note the characteristic biphasic linear transition with a unique inflection point for each peptide.

smaller molar ellipticity of PR1 and PR3 indicates shorter helices and/or larger deviation from the conformation of PPII helix in PR2. It is noted that the molar ellipticity of PR is near the arithmetic mean of PR1, PR2, and PR3, indicating little interactions among the three open PPII helices.

Upon thermal titration, ellipticity at 223 nm of all peptides decreases linearly, with two distinct slopes and therefore displays the same biphasic transition as polyproline (cf. Figure 2, panel B), albeit with transition temperatures at 55, 52, 58, and 40 °C for PR, PR1, PR2, and PR3, respectively (Figure 4). The significantly lower transition temperature of PR3 (40 °C) as compared to the ~50 °C transition temperatures of PR, PR1, PR2, and polyproline suggests again that PR3 may contain a less perfect or less stable PPII helix.

NMR Sequential Assignments for the PEVK Peptides. For 2D NMR data analysis, the standard method described by Wüthrich (*29*) was used to carry out the sequential assignment of all the proton resonances of the PEVK peptides (PR, PR1, PR2, and PR3). TOCSY spectra were used to identify spin systems, and NOESY and ROESY spectra were used to obtain interresidue connectivities and to distinguish equivalent spin systems. Our strategy to make clear assignments followed three steps. First, we examined the αH/NH fingerprint regions of the TOCSY spectra (Figure 5, panel A, and Figure 6, panels A, C, and E), which showed sixteen cross-peaks for PR, six cross-peaks for PR1, seven cross-peaks for PR2, and five cross-peaks for PR3. These signals matched the numbers of the residues, which have amide

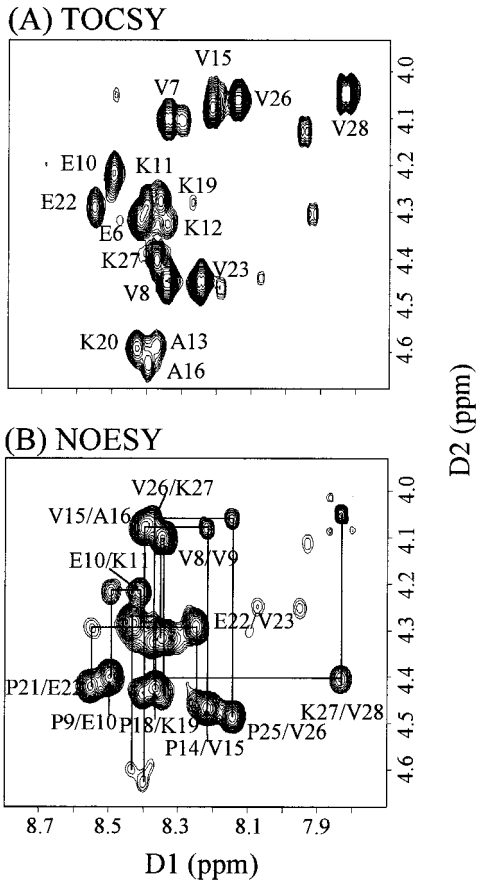

FIGURE 5: 2D NMR and assignment of PR. 2D NMR of PR peptide (13 mg/mL) in 10 mM KPi, pH 6.9, 25 °C was measured and assigned. (A) Expanded TOCSY region for the PR peptide showing αH-NH through bond connectivity; the assignments of the αH-NH cross-peaks of PR are indicated by the sequential number of the corresponding amino acid. (B) Expanded NOESY region for the PR peptide showing αH-NH through space connectivity, of which well-resolved cross-peaks are labeled.

protons. Since proline residues do not contain amide proton and the amide proton of the N-terminal residue is always absent, PR1, PR2, and PR3 peptides should have six, seven, and five amide protons, respectively, which match the number of the cross-peaks in the TOCSY spectra. For PR peptide, only sixteen amide protons were observed, although it should have eighteen amide protons. These two missing amide protons are assigned to one Glu and one Lys in the N-terminal of the peptide, presumably due to their flexibility. With TOCSY NH to αH couplings as starting points, sixteen spin systems (for PR), six spin systems (for PR1), seven spin systems (for PR2), and five spin systems (for PR3) were identified. They were 6 Val, 3 Glu, 2 Ala, and 5 Lys for PR; 2 Val, 3 Glu, and 1 Lys for PR1; 1 Glu, 3 Lys, 2 Ala, and 1 Val for PR2; and 1 Glu, 3 Val, and 1 Lys for PR3, respectively. Second, upon careful sequence examination, several unique amino acid residues were found. For example, within PR2 peptide there is only one Glu residue, which can be assigned unambiguously to residue 10. Furthermore, because one N-terminal Val lacks an amide proton, another Val residue was easily assigned using the amide proton signal as a starting point. Therefore, one is Val8 and another is Val15. Similarly, PR3 peptide contains only one Glu residue, which was assigned to Glu22 and two Lys residues of which only one has amide proton (Lys27). Third, using these unique

Table 1: Resonance Assignment for PR Peptide in 10 mM NaPi, pH 6.9, 25 °C

	NH	αH	βH	others
Pro		4.42	2.45	γCH2 2.05 δCH2 3.44, 3.38
Glu		4.42	1.90, 2.04	γCH2 2.31, 2.45
Pro		4.71	2.30, 2.04	γCH2 1.90 δCH2 3.84, 3.65
Pro		4.44	2.31, 2.05	γCH2 1.91 δCH2 3.83, 3.66
Lys	8.40	4.30	1.81	γCH2 1.43 δCH2 1.73
Glu	8.42	4.32	1.98, 1.92	γCH2 2.25, 2.21
Val	8.33	4.10	2.02	γCH2 0.88
Val	8.34	4.45	2.10	γCH2 0.99, 0.95
Pro		4.40	2.30, 2.04	γCH2 1.91 δCH2 3.91, 3.72
Glu	8.49	4.22	1.99, 1.96	γCH2 2.31, 2.25
Lys	8.41	4.29	1.88	γCH2 1.47 δCH2 1.75 ϵCH2 3.02
Lys	8.34	4.33	1.81	γCH2 1.43 δCH2 1.73 ϵCH2 2.99
Ala	8.37	4.59	1.38	
Pro		4.47	2.37, 2.06	γCH2 1.90 δCH2 3.66, 3.83
Val	8.21	4.08	2.03	γCH3 0.95
Ala	8.40	4.63	1.35	
Pro		4.72	2.37, 2.07	γCH2 1.90 δCH2 3.85, 3.70
Pro		4.43	2.31, 2.06	γCH2 1.90 δCH2 3.84, 3.65
Lys	8.36	4.28	1.83	γCH2 1.37 δCH2 1.74
Lys	8.43	4.59	1.84	γCH2 1.49 δCH2 1.75 ϵCH2 3.02
Pro		4.42	2.30, 2.04	γCH2 1.91 δCH2 3.85, 3.66
Glu	8.55	4.29	1.99, 1.92	γCH2 2.30, 2.24
Val	8.24	4.45	2.08	γCH3 0.99, 0.95
Pro		4.70	2.36, 2.00	γCH2 1.88 δCH2 3.90, 3.70
Pro		4.48	2.30, 2.05	γCH2 1.90 δCH2 3.84, 3.68
Val	8.14	4.06	2.03	γCH3 0.95
Lys	8.37	4.41	1.84	γCH2 1.37 δCH2 1.74 ϵCH2 3.01
Val	7.83	4.05	2.08	γCH3 0.90

assigned residues as starting points, together with the sequential NOE connectivities from ROESY (for PR1, PR2, PR3) or NOESY (for PR) spectra (Figure 5, panel B, and Figure 6, panels B, D, and F), the sequential specific resonance assignments of PR, PR1, PR2, and PR3 could be completed. The sequential NOE connectivities include Hα(i)-NH(i+1) and Hβ(i)-NH(i+1) NOE cross-peaks. For instance, from the α-H of the Val15 of PR2, N-H of the Ala16 was easily found (Figure 6, panel D). Similarly, the entire sequences of PR, PR1, PR2, and PR3 can be assigned. The complete ^{1}H NMR assignments for PR peptide in NaPi buffer solution are summarized in Table 1.

Secondary Structure Analysis of PEVK Peptides. The deviation of αH chemical shifts from random coil values is a convenient method for establishing secondary structure formation since well-defined chemical shift changes are associated with α-helix and extended β-strand (*30*, *31*). In agreement with the CD data, the PR peptide showed very little evidence of α-helix or β-strand secondary structure in aqueous solution, with $\Delta\delta_{H\alpha}$ values (<0.1 ppm) falling below the chemical shift index proposed for identifying secondary structure in peptides or proteins (Figure 7, panel A). The downfield shift of αH chemical shifts of Glu2, Pro3, Val8, Ala13, Ala16, Pro17, Lys20, Val23, and Pro24 strongly suggests that these residues are distinct. It is likely that these residues are conformationally more rigid than others, because proline sterically restricts the conformation of its preceding residue. It is also clear that $\Delta\delta_{H\alpha}$ values of PR are similar to the corresponding ones in PR1, PR2, and PR3 peptides. As expected, the terminal residues of the truncated peptides deviate significantly from those in PR, revealing the end effect of terminal residues. Overall, the agreement indicates that PR peptide and the truncated peptides adopt similar conformation.

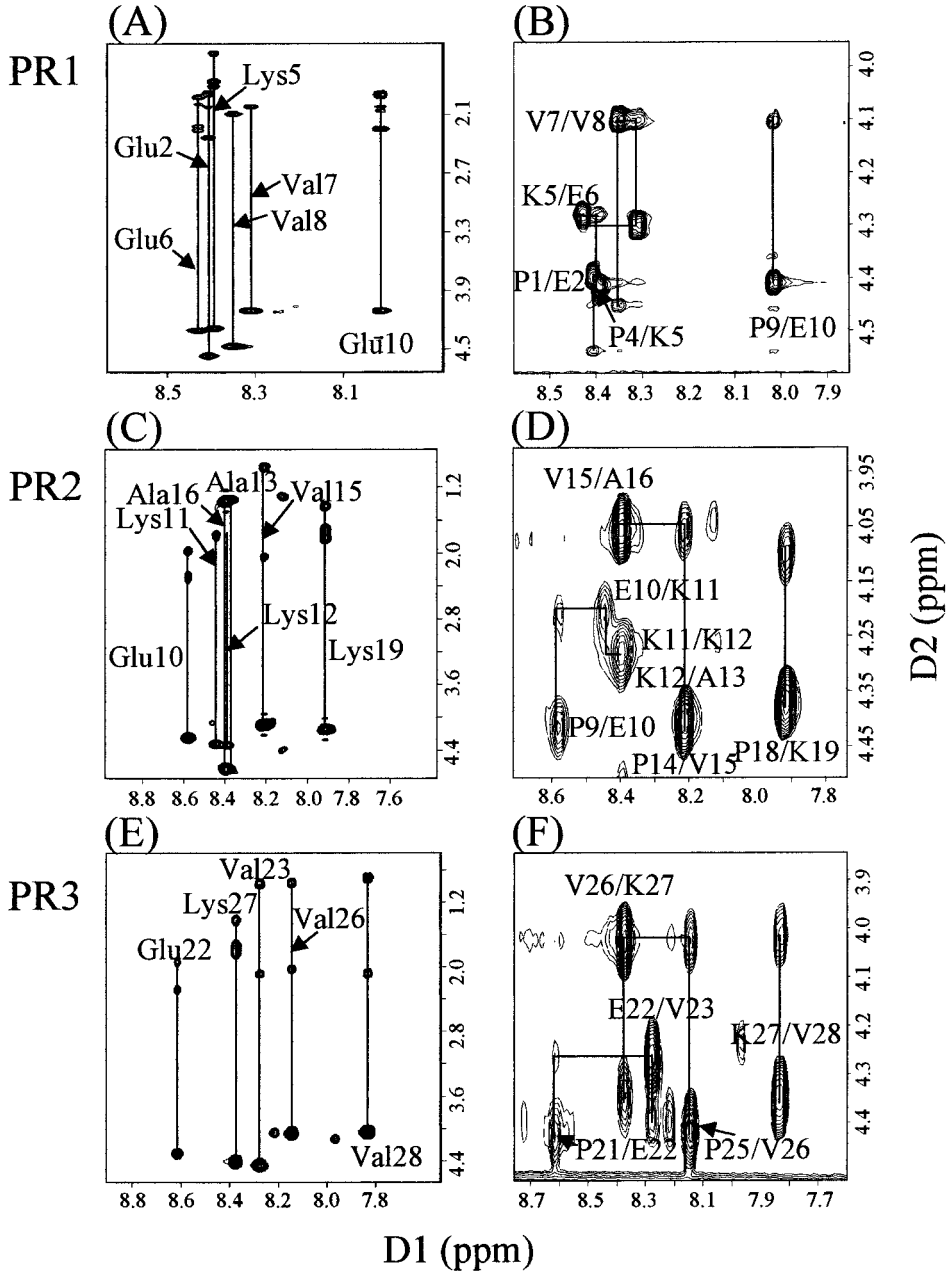

FIGURE 6: 2D NMR and assignment of PR1, PR2, and PR3. 2D NMR of PR1 (7.2 mg/mL), PR2 (9.5 mg/mL), and PR3 peptides (8.3 mg/mL) in 10 mM KPi, pH 6.9, 25 °C were measured and assigned. Left column (panels A, C, and E) displays the expanded TOCSY region for peptides showing spin system for each residue; the assignments are indicated by the sequential number of the corresponding amino acid of PR, (A) PR1; (C) PR2; (E) PR3. Right column (panels B, D, and F) shows expanded NOESY region for the peptides, (B) PR1; (D) PR2; (F) PR3.

The narrow NH chemical shift range (8.6−7.9 ppm) is consistent with solvent-exposed NH (Figure 8) that is not involved in hydrogen bonding. Except for intraresidue NOE peaks, the ROESY and NOESY spectra have few cross-peaks for interresidue NOE, most of which are sequential NOE peaks (Figure 9). The lack of the medium and long distance interresidue NOE signals suggests that the peptides could not adopt α-helix or β-stand secondary structure. These data establish that the PEVK peptides most likely have extended structures, which are also confirmed by the fast H/D exchange rate (all amide protons disappeared in D_2O in 10 min).

The PR peptide signals show negative NOESY cross-peaks with the water line, while all intramolecular NOESY cross-peaks between different protons of PR peptide are positive, as expected for a molecule with slow tumbling rate. All of the ^{1}H NMR lines in the normal 1D spectrum are represented by NOEs in NOESY water line cross section (data not shown), suggesting that all portions of PR peptide molecule are exposed to the solvent, consistent with the extended structure (*32*). However, no tightly bound water molecules could be identified.

The temperature coefficients of all amide resonances are high (>0.007 ppm/K) (Figure 9), indicating that the backbone NH groups are exposed to the solvent and not involved in any intramolecular hydrogen bonding interactions.

The torsion angles ϕ and φ are the essential parameters for defining the backbone conformation of a polypeptide

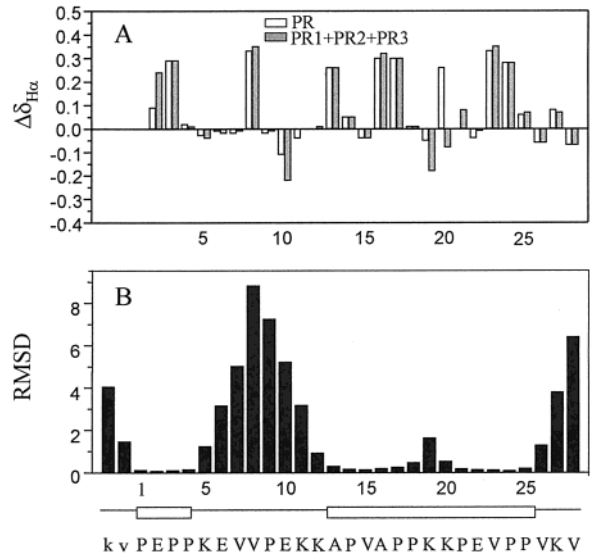

FIGURE 7: Structural characteristics of PR. Amino acid sequence of PR peptide is present in upper cases, with two extra N-terminal residues in lower cases. (A) Differences between the αH chemical shift for the PR in 10 mM KPi, pH 6.9, and those expected for each amino acid residue in a random coil conformation (*31*, *32*) are represented as a function of residue position of the PR peptide. Open column represents the PR peptide, while closed column (gray) shows the combination data of the truncated peptides, PR1, PR2, and PR3. (B) The average RMSD is plotted for each residue. These values were referenced to the mean coordinates by superimposing the backbone atoms of the PR1, PR2, and PR3. Open boxes below panel B indicate well-converged region. Straight lines indicate clusters of RMSD.

chain (*33*). These angles in solution can be detected experimentally by NMR via spin = spin coupling constants, which in case of ^3J coupling constants can be related to specific torsion angles by Karplus relationships (*20*). However, when multiple conformations are adopted, the experimental coupling constants in linear peptides often reflect a population-weighted average over the contributing conformers (*34*). As a result, the interpretation of coupling constants in terms of specific conformations requires caution, especially in the absence of any conformational constraints. The lineshape analysis and measurement of coupling constant at various temperatures have been carried out to examine the reliability of the $^3J_{\alpha N}$ coupling constants (Figure 9).

The intensity ratio between sequential αH-NH(i, i+1) and NH-NH(i, i+1) NOEs is useful as a measure for secondary structure, since it depends on the dihedral angles (ϕ and ψ). Using population-weighted random coil model, Dobson and co-workers predicted that the intensity ratio of αN(i, i+1)/NN(i, i+1) NOEs is about 1.4 for random structure, which is distinctly different from the ratio for extended β-stand conformation (about 55) (*35*). We have carried out an analysis of NOE intensities for PR peptide using NOESY data collected at 298 K. The NH-NH(i, i+1) NOEs are not detected for all residues of PR peptide, while αH-NH(i, i+1) NOEs are medium/strong. This is clearly indicative of a high αN(i, i+1)/NN(i, i+1) intensity ratio, which is consistent with a predominantly extended conformation rather than random coil. The NOE intensity ratio αN(i, i+1)/αN(i, i) provides another piece of evidence of the presence of extended structure in solution. A value of about 2.3 is predicted for the population-weighted random coil model, while values >4 are predicted for a β-stand (*36*). Because of the overlap of the NOE signals, we only measured well-resolved NOE signals for Glu10, Val15, Lys19, Glu22, and Val26. Our data reveal that most of these residues have the αN(i, i+1)/αN(i, i) intensity ratio larger than 4, consistent with a high population of the extended structure through the entire sequence. One sole exception is Glu10 with a ratio of 2.3 (Figure 9), indicating that PR peptide adopts an extended structure with some unordered region located most likely at K5 to K11.

The cis/trans configurations of proline can be distinguished by the difference in interproton distances between the αH of the preceding residues and the proline αH and δH protons (*37*). Short distance (NOE signal) between αH of the preceding residue and δH of the proline is diagnostic for the trans configuration, whereas short distance (NOE signal) between αH of the preceding residues and αH of the proline is diagnostic for the cis configuration. The αδ(i, i+1) NOE cross-peaks in the NOESY spectra strongly indicate that most prolines adopt trans configuration at 5 and 25 °C (Figure 9), which is consistent with the PPII conformation. These sequential NOE connectivities confirm the sequential resonance assignments and support the presence of PPII helix.

Molecular Conformation of PEVK Peptides. The conformational preferences of PEVK peptides can be deduced only from sequential and intraresidue NOE constraints, since there are no long- or medium-range constraints. The strong αδ(i, i+1) NOE cross-peaks between proline and its preceding nonproline residues and between two adjacent proline residues suggest that the backbone ω angles fall at 180°. The strong αN(i, i+1) and αδ(i, i+1) NOE cross-peaks indicate short distance between these protons which are expected in the ψ region of ~120 ± 30°. Since prolines restrict conformational freedom of the residues preceding and following them, the $^3J_{\alpha N}$ coupling constant values of 6.4−7.9 Hz suggest backbone ϕ angle values of nonproline residues flanked by Pro residues of −78 to −90° ± 10°. The backbone ϕ values for prolines are assigned to −60 ± 15°, based on the pyrrolidine ring (*38*). PEVK peptides therefore contain some conformationally restricted regions in proline-rich region such as PxxPP and allows us to build a crude model using backbone parameters within these regions by applying restrained energy minimization and molecular dynamics calculations on structures derived from DGII. The superposition of the backbones of the PEPP region of 11 conformers for PR1, APVAPP region of 8 conformers for PR2 and PEVPP region of 12 conformers for PR3 is shown in Figure 10, panel A. Because of the lack of restraints, the overall convergence of the structures was somewhat low when spread over the entire sequences. The RMSD for the backbone atoms of each peptide are 5.4 ± 1.5 Å for PR1; 3.8 ± 1.2 Å for PR2; and 2.2 ± 0.9 Å for PR3, which are acceptable values given the nature of the unstructured region of the peptides. Significant variations are present in the Lys5−Glu10 region in PR1, Val8−Lys12 region in PR2, and Val26−Val28 in PR3, which are shown by high RMSD in Figure 7, panel B. When backbone superposition was carried out over the restricted regions, the RMSD for the backbone atoms were small, only 0.3 ± 0.12 for APVAPP (Figure 7, panel B). The ϕ and ψ values for each structure set of peptides are plotted in Figure 10, panel B. The ϕ and ψ values of the restricted residues lie within the conformational space of PPII structure.

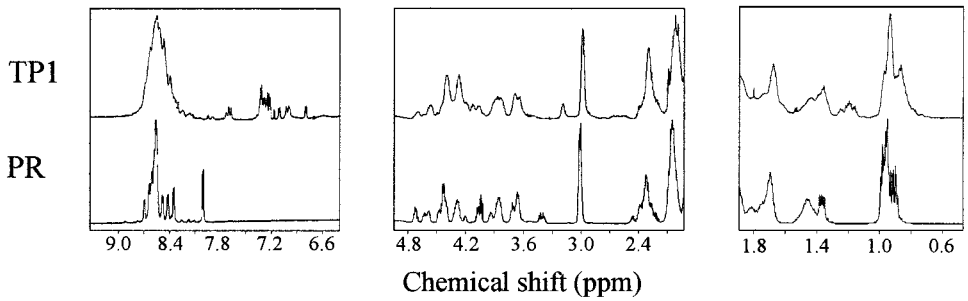

FIGURE 8: The presence of PPII structural motifs in a large PEVK protein TP1. Comparison of ^{1}H spectra for PR peptide and TP1 protein (9.0 mg/mL) in 10 mM KPi, pH 6.9, 25 °C indicates a striking similarity and the presence of PPII motifs in the large 53-kDa protein that contains 16 PR-like motifs.

FIGURE 9: Summary of NMR parameters of PR, PR1, PR2, and PR3. The summary includes sequential NOEs for PR in 10 mM KPi, pH 6.9, the ^3J coupling constants at 5 and 25 °C, and temperature coefficients. The NOE intensities are reflected by the thickness of the lines. When an unambiguous assignment was not possible due to peak overlap, the NOEs are drawn with dots. The intensity ratio of αN(i, i+1)/αN(i, i) is also shown for nonoverlapped residues.

Model Building. To predict the NMR parameters for PPII conformation, we built an ideal PPII conformation model. The interproton distances NH-NH and αH-NH were measured, which gave 4.68 Å for NH-NH and 2.13 Å for αH-NH. The weak NH-NH NOE intensity of 0.8 and strong NOE intensity of 41.8 for αH-NH indicate a high αN(i, i+1)/NN(i, i+1) intensity ratio. The medium range NOEs were not observed, and the αN(i, i+1)/αN(i, i) intensity ratio was predicted to be large. The coupling constant was calculated using the Karplus relationship with ϕ values of −78, which gave a coupling constant of 6.5. All these NMR parameters derived from the PPII model are consistent with our experimental NMR data for the PPII regions in the PR peptide.

A surface model of PR, the 28-module, was built by joining the lowest energy structures of PR1, PR2, and PR3 together and assuming no interpeptide interactions (Figure 11). It is worth noting that most of the charged residues are clustered in the unordered, flexible regions of the module. Three open, rigid PPII helices are deficient in charged residues. Indeed, the longest and perhaps more stable PPII (APVAPP) is a two-turn helix devoid of charges but is flanked on both sides with KKs. PPII in PR1 (PEPP) and PR3 (PEVPP) are shorter, less perfect, and more labile. The presence of negatively charged E in these helices may have contributed to their deformation and affected stability (cf. Figure 4). Furthermore, Pro14 and Pro17 in PR2 are located in a hydrophobic region on the same edge of the PPII helix. This feature further supports the notion that PR2 represents a potential SH3 domain binding motif (*24*).

To summarize, our NMR, CD, and modeling data indicate that many residues in PR peptide are clearly in an open, extended PPII helical conformation and not at all random (Table 2). The distinguishing features are the lack of NOE NN(i, i+1), very large NOE αN(i, i+1)/NN(i, i+1), no medium range NOE αN(i, i+2), positive CD band at 223 nm, and the characteristic Ramachandran space (ϕ and ψ values of −78 and 146, respectively), which shows 4 residues out of 12 for PR1, 6 residues out of 12 for PR2, and 5 residues out of 9 for PR3 are in the PPII helical conformation, respectively. This gives a repeating "PhC" motif for approximately every 10 residues and ~50% of the residues of this fundamental PEVK module fold into PPII-like helices.

NMR of TP1. To evaluate whether PPII helices are also key structural folds in the PEVK protein, we measured 1D ^{1}H NMR spectra for TP1, a 53-kDa expressed protein containing 16 tandem repeats of PEVK modules and nonrepeat human fetal titin PEVK sequences (*11*). As shown in Figure 8, TP1 spectra are consistent with a predominantly open conformation. The high degree of degeneracy and the lack of any upfield-shifted CH_3 resonances indicate the absence of a hydrophobic pocket that is normally associated with globular proteins. Comparison of the spectra for TP1 protein and PR peptide reveals that they are very similar,

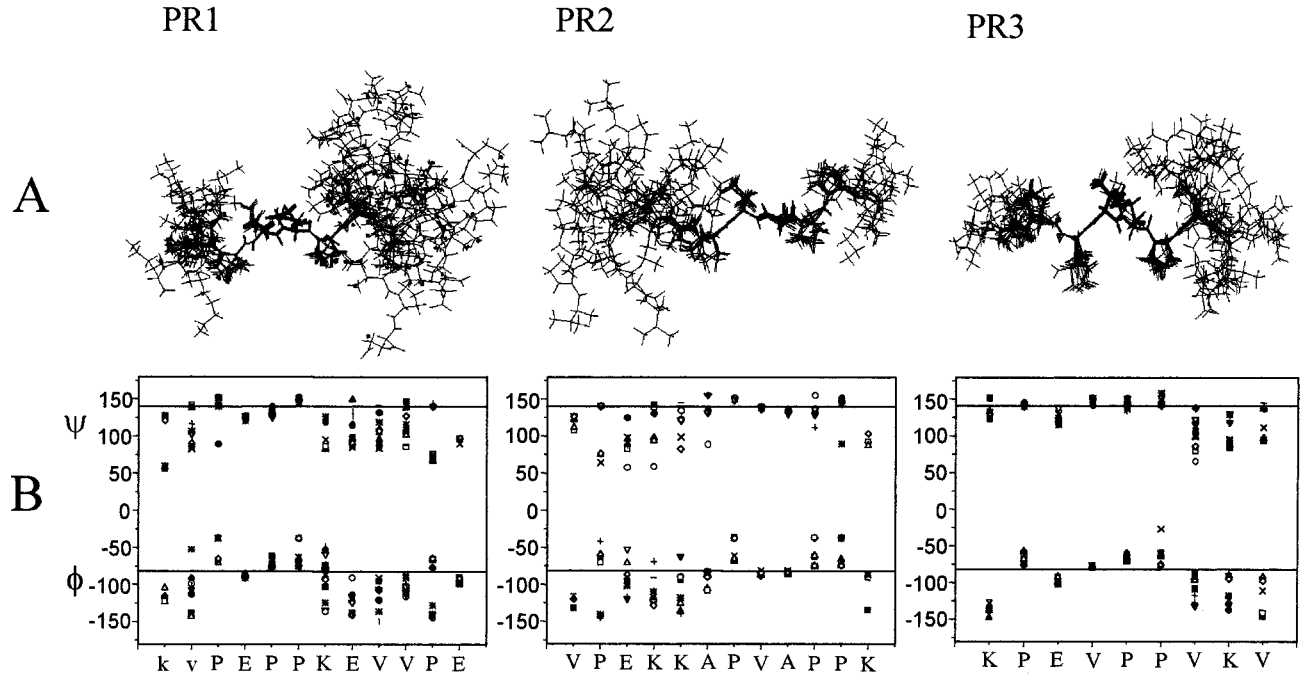

FIGURE 10: Molecular structures of PR1, PR2, and PR3. (A) The superposition of energy-minimized structures for PR1 by superimposing residues Pro1−Pro4; PR2 by superimposing residues Ala13−Pro18; and PR3 by superimposing residues Pro21−Pro25. (B) Backbone dihedral angle (ϕ, ψ) distribution of NMR structures of PR1, PR2, and PR3. Horizontal lines correspond to the canonical (ϕ, ψ) values of the PPII conformation.

Table 2: Distinguishing Features for Random Coil and Extended Structure

	random coil (distribution of φ and ϕ)	extended structure	
		β structure	PEVK (PPII) data
αH chemical shift dispersion (ppm)	within 1 ppm, narrow	wide	narrow
αH chemical shift difference ($\Delta\delta_{\alpha H}$)	($\Delta\delta_{\alpha H}$) < 0.1 ppm	($\Delta\delta_{\alpha H}$) > 0.1 ppm, shift downfield	($\Delta\delta_{\alpha H}$) < 0.1 ppm
NH chemical shift difference ($\Delta\delta_{NH}$)	($\Delta\delta_{NH}$) < 0.2 ppm	($\Delta\delta_{NH}$) > 0.2 ppm, shift downfield	($\Delta\delta_{NH}$) < 0.2 ppm
$^3J_{\alpha N}$ coupling constant	6.5−7.0 Hz, 5.8 Hz for Gly	>8.5 Hz	6.4−7.9 Hz
NOE NN(i, i+1)	observed, medium	no	no
NOE αN(i, i+1)/NN(i, i+1)	2.7 (β) − 1.0 (α), avg 1.4	>55	very large
NOE αN(i, i+1)/αN(i, i)	2.3	>4	2.3−16.6
medium range NOE αN(i, i+2)	observed	no	no
CD	negative band at 196 nm	negative band at 218 nm	negative at 198, positive at 223 nm
Ramachandran (φ and ϕ)	distribution	φ: 90−180; ϕ: −45 ∼ −175	φ: 90−180; ϕ: −45 ∼ −180

except that the peaks are broader for TP1 protein, due to the slower tumbling of a long polypeptide. These data suggest that PR modules are likely to adopt similar "PPII helix and coil" combination as a basic conformational motif structure in the PEVK segments of the titin molecule. Thus, the PR peptide is a functionally relevant structural model for the understanding of the conformational dynamics of the PEVK segment of the elastic titin molecule.

DISCUSSION

Polyproline II Helix as a Structural Motif of PEVK Modules. Our CD and NMR analysis and model building of one representative PEVK module and its subfragments show that in an aqueous environment, this PEVK module may contain three short stretches of open and rigid PPII helices interposed with unordered and presumably flexible structures to give a repeating motif of "polyproline II helix-coil" or "PhC" motif for roughly every 10 residues. Overall, 15 out of 30 residues are in the PPII helical conformation.

The sequence of this and other PEVK modules contains two motifs that are known to promote PPII helix formation and participate in a wide range of protein−protein interactions: the PXXP motif for SH3 domains and the PXY motif for WW domains (*24*, *39*). Studies of the PR2 peptide confirmed our prediction that it would adopt a PPII helix conformation. Indeed, PR2 and a SH3 bound PPII peptide share very similar NMR structures (*40*). The side chains of Pro14 and Pro17 lie on the same side, which stabilize the PPII structure. The similarity in turn suggests that PEVK modules might be targets for SH3 signaling.

CD has proven to be a powerful and discriminating tool in the identification of PPII in PEVK peptides (*41*). The presence of the positive band near 223 nm for PR2 peptide in aqueous solution is clearly indicative of the presence of PPII conformation. This hallmark for PPII conformation is also observed in systemin (*42*), N-terminus of the prion protein (*43*), and histone fragments (*44*). The absence of a positive band near 223 nm in the CD spectra of PR, PR1, and PR3 indicates that the PPII-like conformations deviate from the standard PPII conformation. Since the wavelength of the $\pi-\pi^*$ transition depends on whether the amide is secondary (190 nm) or tertiary as in X-Pro (200 nm), it might serve as a diagnostic for PPII conformation. Moreover, the $n-\pi^*$ transition which has the wavelength around 220 nm

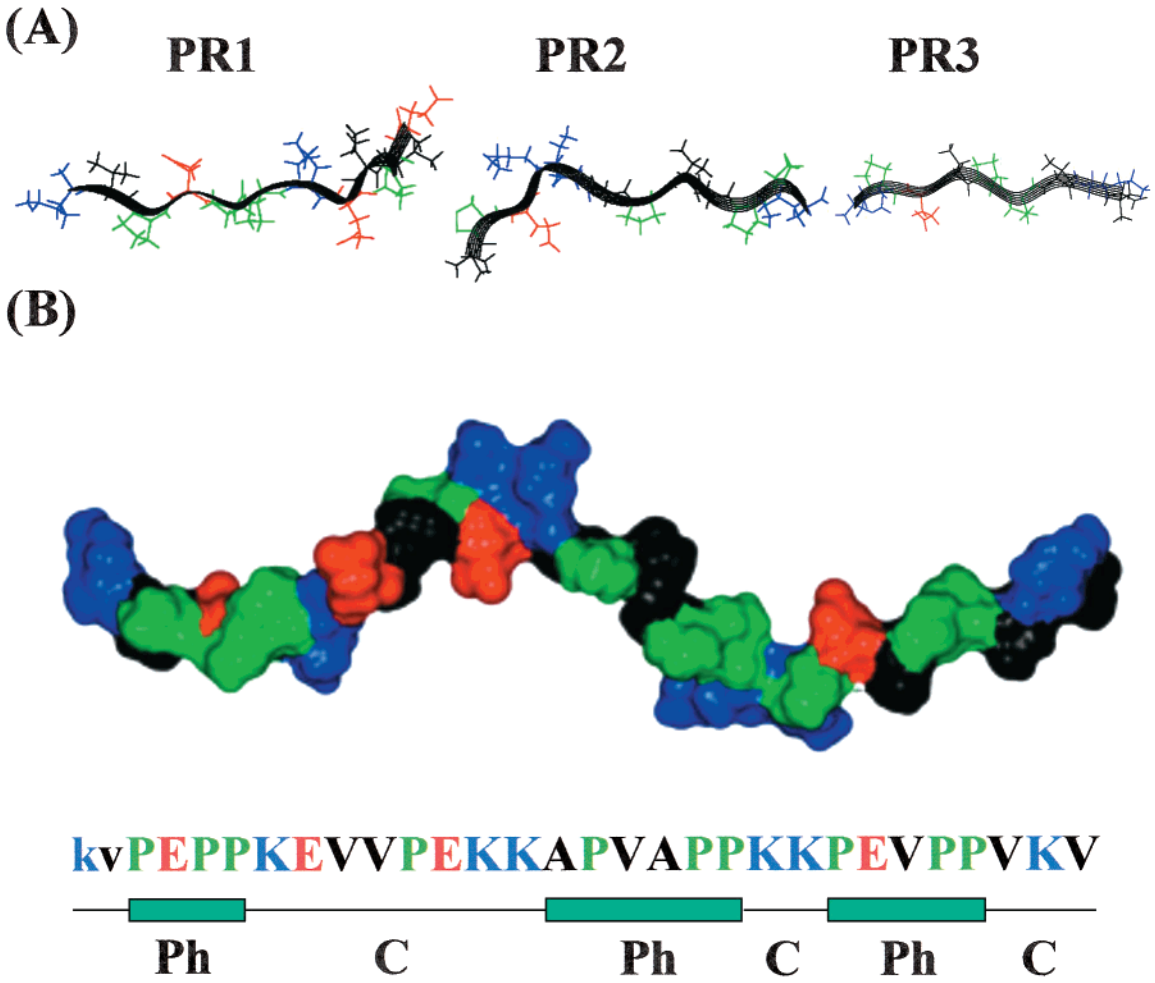

FIGURE 11: Molecular model of the 28-mer PEVK module. (A) Lowest energy structures representing PR1, PR2, and PR3. Lysine, glutamate, and proline residues are indicated in blue, red, and green, respectively. (B) Molecular surface of the structure generated by joining PR1, PR2, and PR3. The surface color is defined according to amino acid residue properties (red, negative charged residue; blue, positive charged residue; and green, proline residue).

could be used to examine the quality of PPII conformation. When the sequence contains more proline residues, this CD band is closer towards 229 nm (*45*), otherwise it moves to lower wavelength (*46*). Also the intensity of this positive band may reflect the stability of the PPII helix. The characteristic biphasic and linear thermal titration curves (by monitoring CD at 223 or 200 nm) and the presence of a transition temperature near 45−65 °C are also important feature of PPII helices (*47*). Since the amide groups in the PPII helix interact with solvent rather than to other peptide groups in the helix, helix formation and disruption are noncooperative. Over a wide temperature range, melting of the PPII helix with increasing temperature to form the truly unordered conformation provides a characteristic linear temperature dependence of the CD. The significantly lower thermal transition temperature and smaller molar ellipticity of PR3 suggest that these parameters are useful quality indices of the PPII helices.

Recent and intense interests in protein folding and protein stability have renewed efforts in characterizing the structures of denatured states of proteins (*48*, *49*). NMR techniques, while widely successful in elucidating native conformations of globular proteins, have met with more limited success in revealing the structure of denatured states that are open and flexible (*41*). This difficulty arises mainly from the limited chemical shift dispersion that results in extreme overlap of the NMR signals and the lack of medium and long distance NOE cross-peaks that are essential for high resolution structure determination. Similar difficulty is also encountered here by us. Our NMR data clearly indicate that it is impossible to determine a unique conformation for PEVK peptide in solution, nor is it meaningful to do so.

It is noted that although several NMR parameters [narrow αH chemical shift dispersion, chemical shift index (CSI) and $^3J_{\alpha N}$ coupling constants] would have, upon casual observations, led to a random coil designation for PEVK, our studies on NOE intensity and structural analysis have ruled out this interpretation. For unordered structures, there is a distribution of ϕ and ψ angles for each residue to give rise to many conformers (*50*). If the interconversion between conformers is fast on the NMR time scale, the experimental NMR data will be averaged, but do not lead to the complete absence of NOEs (*51*, *52*). In fact, the random coil model predicts that all sequential Hα-NH and NH-NH NOEs as well as a number of medium range NOEs are observable (*35*). These NOEs would not be observed for extended structure such as β-strand and PPII, since their interproton distances are larger than 5.5 Å. That the NMR data for PR peptide show no NH-NH NOEs and medium range NOEs such as αN(i,i+2), together with the existence of large NOE intensity ratio αN(i, i+1)/

αN(i, i) for some residues, indicate that PEVK peptide is not completely random and unordered. Instead, there are extended structures such as PPII helices along portions of the PEVK module.

The PEVK peptide shares similar NOE features with another extended structure, the β-strand. A recent molecular dynamics simulation study showed that the behavior of $(Ala)_8$ with the starting conformations of PPII and β were similar, located within the similar region of the Ramachandran diagram (*53*). However, certain NMR parameters of our PEVK peptides (narrow amide proton range, small CSI) distinguish PPII from the β-strand. Therefore, there is no evidence that PEVK peptide contains β-strand.

"PPII Helices-Coil" as a Conformational Motif of PEVK and Functional Implications. Our data indicate that short polyproline type II left-handed helices may well be dispersed throughout the PEVK repeat and superrepeat regions. The broad presence of PPII helices of PEVK region in other muscles is predicted based on the abundance of these PPII motifs in titin PEVK sequences. For example, a search for PxPP, PxxPP, xPxxPP motifs reveals more than 200 sites along the length of the 2176 residues of human soleus titin PEVK (K. Ma and K. Wang, unpublished). These NMR data confirm and extend our earlier proposal that PPII are present in an expressed fragment TP1 from human fetal titin PEVK (*11*). Our earlier estimate of ~13% PPII content in TP1 appears to be an underestimate, since it was calculated based on the much higher molar ellipticity of polyproline standard. It is clear from the present CD studies that individual molar (residue) ellipticities are lower and, moreover, vary with the length and quality of PPII helices.

Since PPII imparts a semirigid, rod-shaped conformation to the PR peptide backbone, PEVK is likely to have an alternating "helix-coil" appearance along the length. These open rigid structures may be sites of protein interactions with, e.g., actin and nebulin as demonstrated by TP1 (*11*), or with perhaps SH3 domains of signaling proteins as predicted by the PR2 conformation.

The tandem repeats of the "PhC" conformational motifs along the length of PEVK may have important structural implications for the understanding of the molecular elasticity of PEVK region of titin (see review by Wang et al., *8*). Our data clearly indicate that the PEVK region is far from random, and the modeling of titin elasticity in this region must now take into consideration the number, distribution, quality, and stability of individual PPII helical region as well as the flexibility and charge interactions of the unordered "coils" region. Elsewhere, we present evidence that the environmental conditions such as temperature, ionic strength, and divalent cations have profound effect on the conformation of PEVK peptides via cis/trans isomerization (Ma et al., manuscript submitted). Significantly, these factors also affect the elasticity of TP1 as measured by stretching single TP1 molecules by atomic force microscopy (*54*). It is conceivable that, *in situ*, PEVK conformation, especially the content and quality of PPII helices, may depend upon the local ion strength, calcium concentration, and intermolecular interaction with other cellular components that in turn modulate PEVK elasticity.

ACKNOWLEDGMENT

K.M. and K.W. thank the Cleveland Center for Structural Biology for the use of NMR spectrometer. We thank Dr. Andrea Sinz for helpful discussion.

REFERENCES

1. Wang, K. (1996) *Adv. Biophys. 33*, 123−134.
2. Horowits, R. (1999) in *Reviews of Physiology Biochemistry and Pharmacology*, Vol 138, pp 57−96.
3. Trinick, J., and Tskhovrebova, L. (1999) *Trends Cell Biol. 9*, 377−380.
4. Wang, K., McCarter, R., Wright, J., Beverly, J., and Ramirez-Mitchell, R. (1991) *Proc. Natl. Acad. Sci. U.S.A. 88*, 7101−7105.
5. Wang, K., McCarter, R., Wright, J., Beverly, J., and Ramirez-Mitchell, R. (1993) *Biophys. J. 64*, 1161−1177.
6. Labeit, S., and Kolmerer, B. (1995) *Science 270*, 293−296.
7. Freiburg, A., Trombitas, K., Hell, W., Cazorla, O., Fougerousse, F., Centner, T., Kolmerer, B., Witt, C., Beckmann, J. S., Gregorio, C. C., Granzier, H., and Labeit, S. (2000) *Circ. Res. 86*, 1114−1121.
8. Wang, K., Forbes, J. G., and Jin, A. J. *Prog. Biophys. Mol. Biol*., in press.
9. Linke, W. A., Ivemeyer, M., Mundel, P., Stockmeier, M. R., and Kolmerer, B. (1998) *Proc. Natl. Acad. Sci. U.S.A. 95*, 8052−8057.
10. Linke, W. A., Ivemeyer, M., Olivieri, N., Kolmerer, B., Ruegg, J. C., and Labeit, S. (1996) *J. Mol. Biol. 261*, 62−71.
11. Gutierrez-Cruz, G., Van Heerden, A., and Wang, K. *J. Biol. Chem.*, in press.
12. Bax, A., and Davis, D. G. (1985) *J. Magn. Reson. 65*, 355−360.
13. Kumar, A., Ernst, R., R., and Wuthrich, K. (1980) *Biochem. Biophys. Res. Commun. 95*, 1−6.
14. Rance, M., Sorensen, O. W., Bodenhausen, G., Wagner, G., Ernst, R. R., and Wuthrich, K. (1983) *Biochem. Biophys. Res. Commun. 117*, 479−485.
15. Bax, A., and Davis, D., G. (1985) *J. Magn. Reson. 63*, 207−215.
16. States, D. J., Haberkorn, R. A., and Ruben, D. J. (1982) *J. Magn. Reson. 48*, 286−292.
17. Shaka, A. J., Lee, C. J., and Pines, A. (1988) *J. Magn. Reson. 77*, 274−293.
18. Otting, G., Widmer, H., Wagner, G., and Wuthrich, K. (1986) *J. Magn. Reson. 66*, 187−193.
19. Dauber-Osguthorpe, P., Roberts, V. A., Osguthorpe, D. J., Wolff, J., Genest, M., and Hagler, A. T. (1988) *Proteins: Struct., Funct., Genet. 4*, 31−47.
20. Karplus, M. (1959) *J. Chem. Phys. 30*, 11−15.
21. Pardi, A., Billeter, M., and Wüthrich, K. (1984) *J. Mol. Biol. 180*, 741−751.
22. Cowan, P. M., and McGavin, S. (1955) *Nature 176*, 501−503.
23. Stapley, B. J., and Creamer, T. P. (1999) *Protein Sci. 8*, 587−595.
24. Ren, R., Mayer, B. J., Cicchetti, P., and Baltimore, D. (1993) *Science 259*, 1157−1161.
25. Ronish, E. W., and Krimm, S. (1974) *Biopolymers 13*, 1635−1651.
26. Rabanal, F., Ludevid, M. D., Pons, M., and Giralt, E. (1993) *Biopolymers 33*, 1019−1028.
27. Arnott, S., and Dover, S. D. (1968) *Acta Crystallogr. B. 24*, 599−601.
28. Naganagowda, G. A., Gururaja, T. L., and Levine, M. J. (1998) *J. Biomol. Struct. Dyn. 16*, 91−107.
29. Wuthrich, K. (1986) *NMR of Proteins and Nucleic Acids*, Wiley, New York.
30. Wishart, D. S., Sykes, B. D., and Richards, F. M. (1992) *Biochemistry 31*, 1647−1651.

31. Wishart, D. S., and Sykes, B. D. (1994) *Methods Enzymol. 239*, 363−392.
32. Otting, G., Liepinsh, E., and Wuthrich, K. (1991) *Science 254*, 974−980.
33. Ramachandran, G. N., Ramadrishnan, C., and Sasisekharan, V. (1963) *J. Mol. Biol. 7*, 95−99.
34. Dyson, H. J., and Wright, P. E. (1991) *Annu. Rev. Biophys. Biophys. Chem. 20*, 519−538.
35. Fiebig, K. M., Schwalbe, H., Buck, M., Smith, L. J., and Dobson, C. M. (1996) *J. Phys. Chem. 100*, 2661−2666.
36. Sharman, G. J., and Searle, M. S. (1998) *J. Am. Chem. Soc. 120*, 5291−5300.
37. Hinck, A. P., Eberhardt, E. S., and Markley, J. L. (1993) *Biochemistry 32*, 11810−11818.
38. MacArthur, M. W., and Thornton, J. M. (1991) *J. Mol. Biol. 218*, 397−412.
39. Sudol, M. (1996) *Prog. Biophys. Mol. Biol. 65*, 113−32.
40. Feng, S., Chen, J. K., Yu, H., Simon, J. A., and Schreiber, S. L. (1994) *Science 266*, 1241−1247.
41. Siligardi, G., and Drake, A. F. (1995) *Biopolymers 37*, 281−292.
42. Toumadje, A., and Johnson, W. C., Jr. (1995) *J. Am. Chem. Soc. 117*, 7023−7024.
43. Gill, A. C., Ritchie, M. A., Hunt, L. G., Steane, S. E., Davies, K. G., Bocking, S. P., Rhie, A. G. O., Bennett, A. D., and Hope, J. (2000) *EMBO J. 19*, 5324−5331.
44. Makarov, A. A., Lobachov, V. M., Adzhubei, I. A., and Esipova, N. G. (1992) *FEBS Lett. 306*, 63−65.
45. Petrella, E. C., Machesky, L. M., Kaiser, D. A., and Pollard, T. D. (1996) *Biochemistry 35*, 16535−16543.
46. Drake, A. F., Siligardi, G., and Gibbons, W. A. (1988) *Biophys. Chem. 31*, 143−146.
47. Makarov, A. A., Esipova, N. G., Lobachov, V. M., Grishkovsky, B. A., and Pankov, Y. A. (1984) *Biopolymers 23*, 5−22.
48. Kortemme, T., Kelly, M. J., Kay, L. E., Forman-Kay, J., and Serrano, L. (2000) *J. Mol. Biol. 297*, 1217−1229.
49. Yi, Q., Scalley-Kim, M. L., Alm, E. J., and Baker, D. (2000) *J. Mol. Biol. 299*, 1341−1351.
50. Smith, L. J., Fiebig, K. M., Schwalbe, H., and Dobson, C. M. (1996) *Fold Des. 1*, R95−106.
51. Neri, D., Billeter, M., Wider, G., and Wuthrich, K. (1992) *Science 257*, 1559−1563.
52. Logan, T. M., Theriault, Y., and Fesik, S. W. (1994) *J. Mol. Biol. 236*, 637−648.
53. Sreerama, N., and Woody, R. W. (1999) *Proteins 36*, 400−406.
54. Jin, A. J., Forbes, J. G., and Wang, K. (2000) *Biophys. J. 78*, 381A.

BI0022792